communications biology

A Nature Portfolio journal

Article

https://doi.org/10.1038/s42003-025-07600-3

A hammerhead ribozyme selects mechanically stable conformations for catalysis against viral RNA

Man Lu[1,7], Zhiqiang Cao[1,7], Luoan Xiong[2], Hongying Deng[3], Kangkang Ma[1], Ning Liu[4], Yanding Qin[5], Shen-Bo Chen[6], Jun-Hu Chen[6], Yao Li[2] ✉, Yijin Liu[3] ✉ & Zhongbo Yu[1] ✉

Ribozymes, widely found in prokaryotes and eukaryotes, target nucleic acids and can be engineered as biotechnical tools or for gene regulation or immune therapy. Among them, hammerhead is the smallest and best characterized ribozyme. However, the structure and biochemical data of ribozymes have been disagreed on, making the understanding of its catalysis mechanism a longstanding issue. Particularly, the role of conformational dynamics in ribozyme catalysis remains elusive. Here, we use single-molecule magnetic tweezers to reveal a concerted catalysis mechanism of mechanical conformational selection for a mini hammerhead ribozyme against a viral RNA sequence from the SARS-CoV-2. We identify a conformational set containing five mechanical conformers of the mini ribozyme, where magnesium ions select the active one. Our results are supported by molecular dynamics simulations. Our understanding of the RNA catalytic mechanism will be beneficial for ribozyme's biotechnological applications and as potential therapeutics against RNA viruses.

Small ribozymes are catalytic RNAs less than 200 nucleotides in length, evolutionarily coming from the RNA world and divergently existing in life such as viroids, Schistosoma, newts, and plants[1–5]. In human and mammals, ribozymes are generally embedded within long noncoding RNAs, creating catalytic RNA domains in lncRNAs[6]. The RNA cleavage activities of ribozymes can be performed in both cis and trans fashions, playing roles in gene regulation and immune responses[7,8]. For instance, a ribozyme from human *ALU* element has been discovered to undergo self-cleavage during T-cell activation[9]. Another example is the hammerhead ribozyme, which regulates the expression of specific CLEC2 proteins by cleaving their corresponding mRNAs, thereby triggering the natural killer immune response in various mammals[10]. In addition to directly cleaving RNA substrates, bacterial ribozymes can also interact with RNA-activated proteins to stimulate the human innate immune responses[11]. Because of their short coding sequence and high degree of modularity, ribozymes have been biotechnologically engineered as tools for potential therapeutic applications, selectively inducing gene activity in target RNA-expressing cells[12–14]. Additionally, ribozymes can be constructed as logic operators by connecting them with different aptamer domains, serving as endogenous spatial and temporal gene regulators in both prokaryotes and eukaryotes[15,16].

Ribozymes exhibit the remarkable ability to perform site-specific cleavage of RNA phosphodiester backbones by activating a 2′ hydroxyl group and facilitating an attack on the neighboring phosphate. This enzymatic process leads to the formation of a 5′ hydroxyl group and a 2′-3′ cyclic phosphate[17,18]. Despite their shared catalytic function, ribozymes display considerable structural diversity. In both prokaryotes and eukaryotes, structured RNAs within the untranslated regions of genes can show either contiguous or discontinuous configurations while maintaining their catalytic activity. The hammerhead ribozyme, a well-studied example, remains a subject of scientific investigation due to the unresolved relationship between its structure and function. The theory of conformational selection is believed to play a dominant role in this relationship[19,20]. Despite an extensive collection of X-ray crystal structures and NMR solution structures, fully understanding the correlation between the ribozyme behavior and catalytic theory remains elusive.

[1]State Key Laboratory of Medicinal Chemical Biology, Frontiers Science Center for Cell Responses, College of Pharmacy, Nankai University, Tianjin, China. [2]School of Physics and Key Laboratory of Functional Polymer Materials of Ministry of Education, Nankai University, and Collaborative Innovation Center of Chemical Science and Engineering, Tianjin, China. [3]State Key Laboratory of Medicinal Chemical Biology, Frontiers Science Center for New Organic Matter, and College of Pharmacy, Nankai University, Tianjin, China. [4]State Key Laboratory of Medicinal Chemical Biology, Nankai University, Tianjin, China. [5]College of Artificial Intelligence, Nankai University, Tianjin, China. [6]National Institute of Parasitic Diseases, Chinese Center for Diseases Control and Prevention (Chinese Center for Tropical Diseases Research), National Health Commission of the People's Republic of China (NHC) Key Laboratory of Parasite and Vector Biology, WHO Collaborating Center for Tropical Diseases, National Center for International Research on Tropical Diseases, Shanghai, China. [7]These authors contributed equally: Man Lu, Zhiqiang Cao. ✉e-mail: liyao@nankai.edu.cn; yvliu@nankai.edu.cn; zyu@nankai.edu.cn

The hammerhead ribozyme consists of three helices and a junction, with a conserved core of nucleotides essential for its cleavage function. The overall conformation of the hammerhead ribozyme adopts a Y-shaped structure, with two helices arranged in a stacked manner while the third helix diverges from this axis along with the junction. The three-helical junction plays a crucial role in organizing the packing of RNA helices in three-dimensional space, facilitating tertiary contacts among different helical domains[21–23]. The binding of divalent ions and RNA substrates enhances the structural flexibility of the hammerhead ribozyme, contributing to both conformational changes and catalytic activity. This structural flexibility is hypothesized to enable allosteric regulation of ribozyme activity[16,17], but it also poses challenges in elucidating the intricate relationship between their structures and functions.

Although careful considerations have been made in designing the small ribozyme, such as positional entropy, structural flexibility, and related measures, it is often observed that a well-predicted hammerhead motif does not function as expected in biochemical cleavage assays. Conversely, a well-functioning hammerhead motif often exhibits conformations that differ from those predicted by comparing NMR data and crystal structures. The discordance between ribozyme structure and function has hindered the use of ribozymes as a viable drug against the severe acute respiratory syndrome coronavirus 2 (SARS-CoV-2) during the outbreak of coronavirus disease-2019 (COVID-19). This is believed to stem from inconsistencies in the pre-existing conformational ensemble[24].

Unlike X-ray crystallography and NMR techniques, which require synchronized conformations for structure analysis, single-molecule techniques are powerful tools for detecting mixed conformations simultaneously in dynamic systems[25–27]. For example, single-molecule mechanical methods have successfully revealed the conformational ensembles of various RNA structures, such as HIV RNA hairpin, riboswitch aptamers, Zika virus RNA knot, and SARS-CoV-2 pseudoknot[28–32]. Additionally, the kinetic barriers of unfolding the T. thermophila ribozyme have been identified using single-molecule mechanical methods[33]. However, the use of single-molecule mechanical methods to investigate the structure and function of ribozymes for understanding their catalytic mechanisms has not been explored before.

We designed a mini hammerhead ribozyme targeting the genomic sequence of SARS-CoV-2 and employed a single-molecule mechanical technique to investigate the RNA conformations, one at a time. This allowed us to gain valuable insights into the catalytic mechanism while establishing a clear structure-function relationship. Our analysis revealed a group of conformational variations consisting of five mechanical conformers of the ribozyme. It is noteworthy that one of these conformers folds correctively into the active conformation and is not reliant on magnesium ions or substrate RNA. Interestingly, we observed that magnesium ions preferentially favor the active conformation, which exhibits well-folded catalytic core domains. Our results were supported by molecular dynamics (MD) simulations. Additionally, our findings demonstrate that the ribozyme can be induced to accommodate substrate recognition. This serves as strong evidence in support of the theory of conformational selection for biomolecular recognition. The utilization of the single-molecule mechanical approach in this study presents a promising opportunity to acquire an in-depth comprehension of the RNA catalytic mechanism. Furthermore, this technique showcases potential applications in ribozyme-based biotechnology and as potential therapeutics against RNA viruses.

Results

Mechanical unfolding of a hammerhead ribozyme at the single-molecule level

To investigate the catalytic mechanism of ribozymes, we have designed a mini hammerhead ribozyme targeting the genomic sequence of SARS-CoV-2 based on the first reported crystal structure of hammerhead (PDB: 1HMH)[34], featuring conserved junction core domains but varying in the sequences of binding arms and helix II loop. The mini hammerhead ribozyme is Y-shaped, with three helices extending from the junction structure (Fig. 1a and Supplementary Data 1). In the presence of a SARS-CoV-2 RNA, two flanking arms of the ribozyme bind the substrate to form helices I and III with the central stem named helix II. Helices II and III show a tendency to align coaxially with the core, while helix I runs parallel to the major axis of the Y-like structure and is positioned alongside helix II. Domain 1 of the catalytic junction core contains a CUGA loop following the helix I and forms a sharp turn like the uridine turn in tRNA, while domain 2 at the junction is a non-Watson-Crick duplex between helices II and III with a conserved GA/AG mismatch. Hammerhead conformations are known to be divalent ions dependent[35,36]. That is, the three helices are arranged

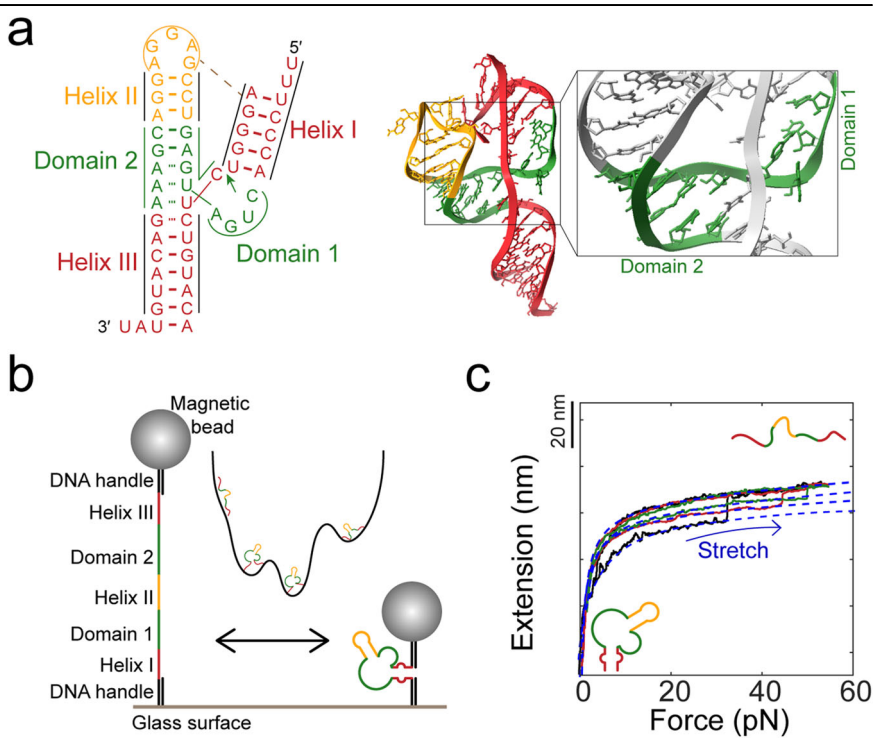

Fig. 1 | The structures of a mini hammerhead ribozyme targeting the genomic RNA sequence of SARS-CoV-2 and the experimental setup for single-molecule studies. a Schematic representation of the mini hammerhead ribozyme highlighting helices I–III and domains 1–2 (left), alongside the 3D structure obtained from molecular dynamics simulations (right, Supplementary Data 1). The green arrow marks the cleavage site. **b** A schematic illustration of the folding and unfolding experiment using single-molecule magnetic tweezers. A colored ribozyme strand is flanked by double stranded DNA in black. The ribozyme is fully unfolded at a high force, but it folds when the forces decrease. The conformational space of the ribozyme is depicted in an energy landscape. **c** Typical force-extension curves (solid lines) in 100 mM NaCl fitted with a Worm-Like-Chain model (blue dashed lines)[30,53].

equidistant around the catalytic core without a defined global fold at low concentrations of divalent ions, whereas the structure assumes a Y-like conformation at high divalent concentrations[36–38]. This renders the junction core structure highly dynamic with tertiary interactions in solution[39–41], suggesting that multiple conformers may exist. The three helices involved in substrate binding need not be conserved if they are satisfactorily base paired for efficient binding.

To examine the ribozyme's conformations, we used the mini hammerhead in conjunction with magnetic tweezers assays, a popular single-molecule mechanical technique[42–44]. Our experimental setup utilized a DNA-RNA-DNA (DRD) design with the mini hammerhead ribozyme sandwiched between two DNA handles (Supplementary Table 1 and Supplementary Fig. 1). Although the ribozyme is positioned between the two DNA handles, it remains sufficiently exposed and accessible to the RNA substrate, as revealed by AFM imaging (Supplementary Fig. 2). The DRD construct was modified with biotins at one end and digoxigenins at the other end to facilitate a strong binding affinity. The DRD construct was anchored to a glass bottom covered with anti-digoxigenins, while a streptavidin-coated bead bound the DRD construct via interactions with biotins, a conventional way to manipulate single RNA molecules[25,31,45]. By applying forces to the DRD construct using magnetic tweezers, we were able to mechanically fold and unfold the ribozyme (Fig. 1b).

Under strong forces, the ribozyme can be extended to a linear conformation. In the absence of a SARS-CoV-2 RNA and divalent ions, we studied the unfolding events of the ribozyme by collecting force-extension curves in a buffer containing 100 mM NaCl. The force-extension curves begin at high forces where the ribozyme is fully unfolded and stretched to a linear form. As the forces decrease to zero at a rate of 0.45 pN s^{-1}, the linearized ribozyme is allowed to relax for 45 s to promote folding. Upon increasing forces from zero, the curve initially follows the folding trajectory until a critical unfolding force is reached, at which point the ribozyme exhibits cooperative unfolding with a forward jump in extension (Fig. 1c). Overlapping force-extension curves revealed multiple unfolding events with varying sizes and forces, indicating the presence of multiple isomers in the ribozyme's conformational space.

The ribozyme folds into conformations with distinct mechanical stabilities

We examined the conformations of the mini ribozyme by measuring the unfolding changes of extensions and forces at the single-molecule level. The force-extension distributions revealed complex shapes of a Gaussian mixture, suggesting that the ribozyme exists in multiple conformations, although it mostly triggers one-step-only unfolding events (Fig. 2a and Supplementary Table 2). Three Gaussians provided the best fit to the distribution of changes in unfolding extension, indicating three conformations of the ribozyme. Based on the basic hammerhead structure of the mini ribozyme, the shortest changes in extension (6.8 ± 0.5 nm) corresponded to unfolding of the stem-loop of the ribozyme helix II (Fig. 2b, yellow) and were named α conformational set. The longest changes in extension (23 ± 5 nm) matched the unfolding of the fully folded hammerhead, including tertiary interactions involving helices I and III in the absence of the RNA sequence of SARS-CoV-2 (Fig. 2b, red) and were named γ conformational set. The intermediate changes in extension (13.6 ± 0.8 nm) corresponded to the unfolding of helix II as well as the core domains (Fig. 2b, green) and were thus named β conformational set. As the unfolding events are primarily cooperative and occur mainly in a single step rather than sequential steps, the ribozyme must fold into multiple isolated wells in an energetic landscape.

Remarkably, the analysis of the unfolding forces identified mechanical subsets of the ribozyme conformations measured by extensions. Except for the unfolding force distribution corresponding to the shortest extension changes (i.e., α set, Fig. 2c, left), both force distributions, that correspond to intermediate and longest extension changes, displayed two distinct peaks (Fig. 2c, middle and right). The presence of two critical unfolding forces for the same conformational set suggests the existence of two mechanical

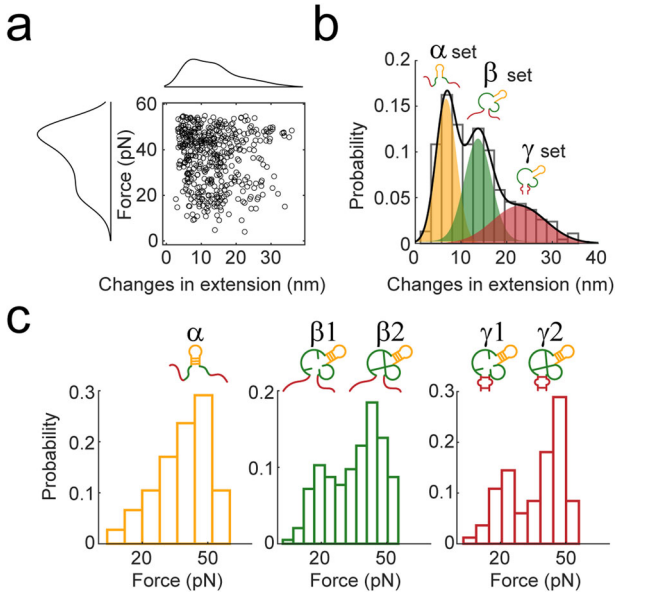

Fig. 2 | Mechanical conformers of the mini hammerhead ribozyme. a Force-extension distribution of the ribozyme unfolding events. The histogram at the top represents the changes in extension during unfolding, while the left histogram shows the distribution of unfolding forces. A total of 462 unfolding events from 263 ribozyme molecules were analyzed, with buffer containing 100 mM NaCl in the absence of substrate RNA and divalent ions. **b** Gaussian mixture modeling of the force-extension distributions. The distribution of extension changes is fitted with three Gaussians. Cartoons illustrate the conformational sets of the ribozyme. **c** Three unfolding force distributions are separated according to their corresponding peaks in the distribution of extension changes. Mechanical conformational subsets are indicated by color codes and cartoons. Left, 180; middle, 187; right, 95 data points.

subsets with identical length. To differentiate between the β subsets, we assigned the labels β1 and β2, while for the fully folded γ subsets we used the labels γ1 and γ2, respectively (Fig. 2c). The stability of conformational states were summarized in Supplementary Table 3. As the probabilities of the occurrence of the two force peaks are approximately equal, it appears that isomerization among folded conformations of the hammerhead ribozyme is common.

Using all-atom MD simulations[46–48], we further revealed that in the mini ribozyme γ conformation, helices I and III can either directly interact or both engage with the core domains (Supplementary Fig. 3 and Supplementary Data 2–5). We predict that the hammerhead is self-inhibited based on our observation of the γ conformation of the ribozyme in the absence of a substrate RNA. This is because the enzyme folding, involving helix I and III domains, may hinder their accessibility for target RNA recognition. As expected, the ribozyme was unable to fully cleave its target RNA substrate in a bulk test at 37 °C after incubation for two hours (Supplementary Fig. 4).

Magnesium ions select the mechanically more stable conformation of the ribozyme

Divalent metal ions play a crucial role in the proper folding and catalysis of hammerhead ribozymes, and both their structures and functions are highly sensitive to these cations[49]. Magnesium ions, in particular, are widely considered as the physiologically relevant ion that can activate the catalytic activity of hammerhead ribozymes[35,41]. We conducted MD simulations under both calcium and magnesium ion conditions. Our results, observed over a 100 ns time scale, indicate that the mini ribozyme remains relatively rigid at the helix II domain (Supplementary Fig. 5 and Supplementary Data 6–11). The conformational dynamics primarily occur within the core domains, especially at the catalytic bases and in the interactions between helix I and helix III. Overall, we found that the mini ribozyme exhibits more dynamic conformations in the presence of magnesium ions compared to

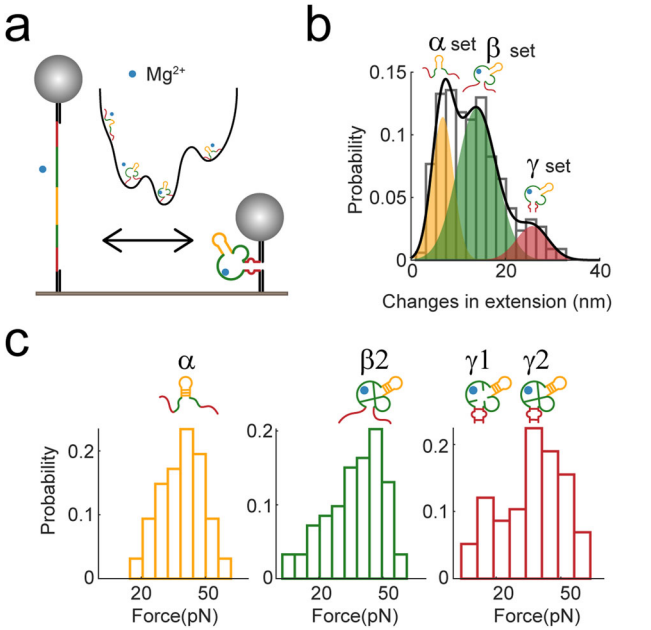

Fig. 3 | The role of magnesium ions in selecting ribozyme conformations. a The setup of the single-molecule conformational selection experiments by magnesium ions. **b** The distribution of extension changes upon unfolding the ribozyme is shown for $n = 339$ from 209 ribozyme molecules in the presence of magnesium ions (sphere). **c** The unfolding force distributions are color-coded and separated based on their corresponding peaks in the extension change distribution, as illustrated by the cartoons. Left, 128; middle, 159; right, 52 data points.

calcium ions. Based on these findings, we chose to use magnesium ions in our single-molecule mechanical assays to further investigate the dynamics of hammerhead ribozymes.

We observed that magnesium ions have a significant impact on the isomerization of the ribozyme. In the presence of 10 mM $MgCl_2$, but in the absence of the substrate RNA, we conducted force-extension assays to fold and unfold the ribozyme strand (Fig. 3a). When compared to that in the absence of magnesium ions, the overall shape of the extension distribution remained similar (Figs. 3b vs 2b), with three peaks of changes in extension almost identical for both conditions. We found that the rupture force for the shortest α conformation set did not respond to magnesium ions, which reflects its helix nature and confirms our initial assignment of helix II structure (Fig. 3c). We also found that magnesium ions do not affect the global structure of the mini hammerhead ribozyme because the unfolding forces for the γ structures remained unchanged. Our theory is thus reaffirmed that the γ conformation set is locked by tertiary interactions, and the core domains are buried inside. However, the unfolding force distribution for the β conformation set showed a single β2 peak, unlike in the absence of magnesium ions when two β peaks were clearly observed. Our results suggest that magnesium ions modulate the isomerization of the local β structure and selectively stabilize it in a higher-rupture force conformational subset. As magnesium ions interact with the core domains, they most likely select the mechanically more stable conformational subset of those domains, causing a shifted equilibrium of the conformers.

To test the impact of sequence changes on the ribozyme, we designed a tiny ribozyme with the sequence 5′-UUCCCACUGAUGAGACUG GACGAAAGACAUGUAU. Both this tiny ribozyme and the original mini ribozyme target the RNA sequence 5′-ACAUGUCUCUGGGA of SARS-CoV-2. However, the tiny ribozyme features a shorter helix II stem and a longer loop compared to the mini ribozyme (Supplementary Fig. 6a).

Using single-molecule mechanical assays in the absence of magnesium and RNA substrate, we observed that the tiny ribozyme exhibits four mechanical conformations with two distinct extension changes (Supplementary Fig. 6b, c). This observation supports our previous finding that ribozymes can adopt conformations with varying mechanical stabilities. In contrast, the mini ribozyme displays five mechanical conformations with three distinct extension changes, likely due to the differences in the helix II stem length, which may influence the adjacent core domains and affect the number of mechanical conformations.

Upon adding 10 mM magnesium, the tiny ribozyme continued to display four mechanical conformations with two extension changes (Supplementary Fig. 6d, e), but there was a notable decrease in the population exhibiting the longer extension change (Supplementary Fig. 6b vs 6d, blue). Similarly, in the mini ribozyme, the population with the longest extension change also decreased (Figs. 3b vs. 2b). The longer extension changes observed in mechanical unfolding assays are indicative of long-range domain-domain interactions. The reduced populations suggest that magnesium facilitates further folding of the inner core domains, potentially disrupting these interactions and resulting in fewer conformations involving long-range domain-domain interactions.

Furthermore, for the tiny ribozyme, the two mechanical conformations with short extension changes exhibited different distributions before and after the addition of magnesium. Post-magnesium addition, the population of the weaker mechanical conformation decreased, resulting in a relative increase in the stronger mechanical conformation (Supplementary Fig. 6c vs 6e, arrows in the right panels). This observation is consistent with findings for the mini ribozyme, suggesting that magnesium ions selectively stabilize the mechanically stronger conformations, thereby shifting the equilibrium toward these more stable states. These results demonstrate the influence of sequence variations on the folding and mechanical properties of ribozymes, highlighting the role of specific structural elements in ribozyme function.

The self-inhibited ribozyme can recognize its substrate

The γ conformations of the ribozyme, which do not include substrate RNA, are inhibited due to tertiary interactions involving helix I and III. To assess the ribozyme's catalytic function, we introduced the genomic RNA sequence of SARS-CoV-2 in the presence of magnesium ions (Fig. 4a). Considering that the catalysis rate of the mini ribozyme is much faster (at the order of ~800 min^{-1}) than our single-molecule unfolding manipulation (~1 min^{-1}), we expected to observe the aftermath of the cleavage reaction[50,51]. Remarkably, the longest extension γ peak disappeared in the resulting distribution (Fig. 4b), which contrasted with the distribution without the substrate RNA. The only remaining extension peaks were the α and β structures, or the shortest and intermediate extensions, indicating that the self-inhibited ribozyme releases the helix I and III domains for recognizing the genomic RNA substrate of SARS-CoV-2. In this setup, the γ conformations of the ribozyme completely unfolded in the presence of the genomic RNA of SARS-CoV-2, indicating highly efficient, or 100% efficient, substrate binding. Furthermore, rupture force distributions in the presence of magnesium ions and substrate RNA indicated the presence of the α and β2 conformations (Fig. 4c). This suggests that the mechanically more stable conformation, β2, rather than β1, is responsible for the ribozyme's catalytic activity.

The efficient RNA cleavage was further supported by the magnesium depletion assay (Fig. 4d, e), which corroborated our interpretation. The force distribution revealed the presence of β1 and β2 conformations, indicating that the mechanical stability of the ribozyme depends primarily on its core domains. The equilibrium among different conformational sets can be modulated by conformational selection through the addition or removal of magnesium ions. Furthermore, the collision between the ribozyme strand and the substrate RNA induces conformational changes that facilitate enzyme-substrate recognition, and primarily affect the helix I and III domains rather than the catalytic core domains.

To further understand the function of the core domains, we designed an inactive mini ribozyme with the sequence 5′-UUUCCCACU GAU**dG**AGUCCGAGGAGGACGAAAGACAUGUAC (Supplementary Fig. 7a and Supplementary Table 1). The inactive ribozyme cannot digest RNA substrate due to the presence of a deoxynucleotide at the catalytic center, indicated by the bold dG in the sequence. However, the inactive

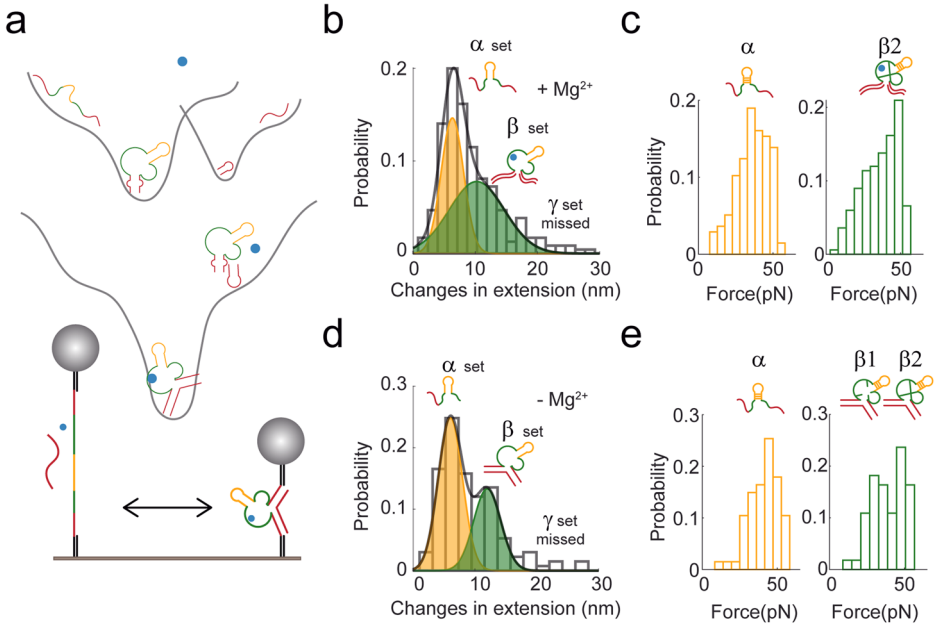

Fig. 4 | The induced-fit recognition between the ribozyme and SARS-CoV-2 RNA. a The setup of the single-molecule induced-fit experiments. **b** The distribution of extension changes upon unfolding the ribozyme in the presence of the RNA sequence of SARS-CoV-2 and magnesium ions. $N = 235$ from 125 ribozyme molecules. **c** The corresponding unfolding force distributions for (**b**). Left, 99; right, 136 data points. **d** The distribution of extension changes upon unfolding the ribozyme in the presence of substrate RNA without magnesium ions. $N = 133$ from 85 ribozyme molecules. **e** The corresponding unfolding force distributions for (**d**). Left, 78; right, 55 data points.

ribozyme retains its ability to recognize and bind the RNA substrate via the helix I and III domains, which are complementary to the RNA substrate.

Single-molecule mechanical assays revealed the presence of α and β conformations but no γ conformations, irrespective of the presence of magnesium (Supplementary Fig. 7b–e). This suggests that the deoxynucleotide dG in the core domain destabilizes the γ conformations, reinforcing our previous findings that the γ conformations are based on tertiary interactions involving the core domains, as evidenced by both our single-molecule assays and MD simulations. Additionally, we observed only one mechanical state of the β conformation in the inactive mini ribozyme, in contrast to the two mechanical states of the β conformation in the active mini ribozyme, suggesting that the mutated guanosine affects interactions with magnesium ions. In the presence of the RNA substrate, the β conformations of the inactive mini ribozyme become shorter, suggesting that the deoxynucleotide dG partially disrupts the core domains (Supplementary Fig. 7f–i).

Discussion

Our approach allowed us to identify a conformation ensemble consisting of five mechanical conformational subsets of the mini ribozyme, with the α subset featuring a folded helix II domain, serving as the basic structure for the ribozyme's conformational ensemble and triggering the enzyme folding process. This ensemble includes the catalytically active conformation of the β2 subset, which is independent of magnesium ions and substrate RNA, and strongly supports the theory of conformational selection for biomolecular recognition. In addition, we observed that magnesium ions bind preferentially to the β2 subset, which possesses well-folded catalytic core domains, thereby demonstrating how a rigid ligand selects its favored enzyme conformation for catalysis. This observation reveals a fundamental mechanism underlying magnesium stimulation of the ribozyme's cleavage activity. Our experiments also showed that the ribozyme is self-inhibited by tertiary interactions involving its helix I and III domains, which can be activated by substrate recognition. Notably, reorganization of the helix I and III domains does not affect the core domains allosterically, indicating that the catalytic core domains are independent of substrate recognition. Therefore, the autonomous dynamic segments of helices I and III exhibit significant potential for the ribozyme to identify various substrate RNAs through mutations, serving as a foundational principle for the advancement of ribozyme-based biotechnology and as potential therapeutics against RNA viruses.

Overall, our findings demonstrated that a concerted mechanism of conformational selection is involved in ribozyme catalysis, with a specific design targeting the digestion of the genomic RNA sequence of SARS-CoV-2. The application of the single-molecule mechanical conformer probing method and the insights gained into the ribozyme mechanism hold promise for future advancements in ribozyme-based diseases control and prevention.

Methods

DNA-RNA-DNA construct

The DRD construct used for single-molecule assays involves five components (Supplementary Table 1 and Supplementary Fig. 1). Two dsDNA handles are generated through PCR using either biotin or digoxigenin modifications. The mini hammerhead ribozyme with flanked DNA at both ends is synthesized through solid-phase synthesis using tert-Butyldimethylsilyl Ethers (t-BDMS) on an ABI 394 synthesizer. Two dsDNA linkers are employed to ligate the DNA handles and the ribozyme together.

AFM imaging

We employed a Multimode 8 AFM instrument manufactured by Bruker (Billerica, USA) and conducted measurements at room temperature (23 °C). The mica surface was prepared by peeling it with tape to ensure flatness and cleanliness. Prior to loading the sample, we mixed the DRD construct with 10 mM $NiCl_2$ in a 40 mM Tris buffer (pH 8.0). We then applied 10 μl of the mixture to the center of the mica surface and allowed it to settle for 3 min. Afterward, the sample was gently rinsed with water and dried using nitrogen gas. For scanning and high-resolution imaging, we used an SNL-10 probe, also from Bruker. The scanning parameters were optimized to ensure the best match between the trace and retrace curves. The scan size was gradually increased from 10 nm to 1000 nm to identify the appropriate range, and the XY offset was adjusted after each scan to explore different areas. Finally, AFM images were analyzed using NanoScope software.

Single-molecule mechanical assays

We employed magnetic tweezers to perform single-molecule mechanical assays as previously described[25,27,44]. The basic buffer used for these assays consisted of 50 mM Tris-HCl, 100 mM NaCl, 1 mM DTT, and 0.003% Tween-20, supplemented with 10 mM $MgCl_2$ as needed. For a buffer without $MgCl_2$, we added 1 mM EDTA. To initiate the assay, we mixed streptavidin-coated beads (Cat#: 65305, M270, Invitrogen, USA) with DRD constructs in a total volume of 60 μl. We then loaded the mixture into a flow cell, with the bottom glass surface coated with anti-digoxigenin antibody

(Cat#: 11093274910, Roche). Using LabView (2017, NI, USA) controlled magnetic tweezers, we applied mechanical forces to unfold and fold the DRD construct, generating force-extension curves which were monitored in real time. The time interval between two sequential force-extension curves is generally set to be longer than 5 minutes, which ensures that a single molecule can refold in the absence of any applied force, allowing us to observe the range of possible conformations the ribozyme can adopt.

MD simulation

We conducted all-atom molecular dynamics (MD) simulations using explicit water molecules (TIP3P model) and the CHARMM36m force field, through the GROMACS 2022.4 software package[46–48]. The MD input files were generated by the CHARMM-GUI web server, with the initial configuration based on the minimum hammerhead ribozyme structure model (PDB:1HMH) but substituting the non-conserved nucleotides according to Fig. 1a. To ensure a neutral system charge, we incorporated 100 mM NaCl using the Monte Carlo method. For simulations including Mg^{2+} ions, we added 1 mM $MgCl_2$, consistent with the concentration used in ribozyme experimental studies. The system was then solvated in a rectangular water box with periodic boundary conditions, having a size of roughly 100 Å × 100 Å × 100 Å, comprising approximately 110,000 atoms. We reduced the system's energy using the steepest descent algorithm within the gromacs2022.4 software package, until reaching a force less than 1000 kJ mol^{-1} nm^{-1}. The system was then equilibrated at 294.15 K for 125 ps using the Nose-Hoover thermostat in the NVT ensemble. Subsequently, we performed production simulations in the NPT ensemble at 294.15 K and 1 atmosphere pressure for 100 ns, using a time step of 2 fs, the Nose-Hoover thermostat, and Parrinello-Rahman barostat. Electrostatic interactions were calculated through the particle mesh Ewald method, while electrostatic and van der Waals interactions were truncated at a range of 12 Å. The bonds consisting of hydrogen atoms were constrained via the LINCS algorithm.

To characterize the different unfolding lengths of the hammerhead ribozyme and determine the free energy difference between various β-conformations, we employed the umbrella sampling technique. The reaction coordinate chosen for this analysis was the distance between the 5′ end and the 3′ nucleotide molecular center-of-mass (COM) of the ribozyme. During the pulling simulation, we applied a spring with a force constant of 1000 kJ mol^{-1} nm^{-2} to restrain the 3′ nucleotide molecular COM of the ribozyme. Additionally, the 5′ nucleotide molecular COM was connected to a spring with the same force constant and subjected to a constant pulling velocity of 0.01 nm ps^{-1}. This pulling simulation was conducted over a period of 2 ns. We obtained a set of trajectories from this simulation, corresponding to 50 umbrella sampling windows. These windows had end-to-end distances ranging from 4.8 nm to 14.8 nm, with an interval of 0.2 nm. Each window was further explored through 10 ns of molecular dynamics simulations, resulting in a total simulation time of 500 ns. To construct the potential of mean force along the reaction coordinate, we utilized the g_wham[52] tool integrated within Gromacs. Moreover, we extracted snapshots of the molecular structures from the MD simulations conducted within each sampling window.

Data analysis

In this study, all single-molecule data were analyzed in MatLab R2022a (Mathworks, USA). We fitted force-extension curves to an extensible Worm-Like-Chain model at an ionic strength of 100 mM NaCl, which closely matched our experimental conditions[30,53]:

$$F = \frac{k_B T}{L_p}\left(\frac{1}{4}\left(1-\frac{x}{L_c}\right)^{-2}\right)+\frac{x}{L_c}-\frac{1}{4}$$

Where L_p is the persistence length, L_c is the contour length, k_B is the Boltzmann's constant, and T is absolute temperature.

Statistics and reproducibility

We measured the changes in extension of cooperative unfolding events in force-extension curves. The distribution of changes in extension was modeled using Gaussian functions. The number of Gaussian functions used for modeling was determined by statistical analysis. Typically, two or three Gaussian functions have been used. The conformations were thus identified by the Gaussian populations, i.e., α, β, and γ sets. For the corresponding force distributions, we statistically assigned the force data to the α, β, or γ sets based on Gaussian probability on a randomized basis. The statistics of single-molecule experiments are summarized in Supplementary Table 2. The data for generating the curves are available in Supplementary Data 12.

Reporting summary

Further information on research design is available in the Nature Portfolio Reporting Summary linked to this article.

Data availability

The authors declare that all data supporting the findings in this study are available within the article, within Supplementary Data files, or from the corresponding author on reasonable request.

Code availability

The codes used in this study are available within Supplementary Data 13.

Received: 17 November 2023; Accepted: 24 January 2025;
Published online: 03 February 2025

References

1. Salehi-Ashtiani, K., Lupták, A., Litovchick, A. & Szostak, J. W. A genomewide search for ribozymes reveals an HDV-like sequence in the human CPEB3 gene. *Science* **313**, 1788–1792 (2006).
2. Roth, A. et al. A widespread self-cleaving ribozyme class is revealed by bioinformatics. *Nat. Chem. Biol.* **10**, 56–60 (2014).
3. Winkler, W. C., Nahvi, A., Roth, A., Collins, J. A. & Breaker, R. R. Control of gene expression by a natural metabolite-responsive ribozyme. *Nature* **428**, 281–286 (2004).
4. Przybilski, R. et al. Functional hammerhead ribozymes naturally encoded in the genome of Arabidopsis thaliana. *Plant Cell* **17**, 1877–1885 (2005).
5. Ferbeyre, G., Smith, J. M. & Cedergren, R. Schistosome satellite DNA encodes active hammerhead ribozymes. *Mol. Cell Biol.* **18**, 3880–3888 (1998).
6. Chen, Y. et al. Hovlinc is a recently evolved class of ribozyme found in human lncRNA. *Nat. Chem. Biol.* **17**, 601–607 (2021).
7. Radakovic, A., DasGupta, S., Wright, T. H., Aitken, H. R. M. & Szostak, J. W. Nonenzymatic assembly of active chimeric ribozymes from aminoacylated RNA oligonucleotides. *Proc. Natl. Acad. Sci. USA* **119**, e2116840119 (2022).
8. Huang, X. et al. Intracellular selection of trans-cleaving hammerhead ribozymes. *Nucleic Acids Res.* **47**, 2514–2522 (2019).
9. Hernandez, A. J. et al. B2 and ALU retrotransposons are self-cleaving ribozymes whose activity is enhanced by EZH2. *Proc. Natl. Acad. Sci. USA* **117**, 415–425 (2020).
10. Martick, M., Horan, L. H., Noller, H. F. & Scott, W. G. A discontinuous hammerhead ribozyme embedded in a mammalian messenger RNA. *Nature* **454**, 899–902 (2008).
11. Hull, C. M., Anmangandla, A. & Bevilacqua, P. C. Bacterial riboswitches and ribozymes potently activate the human innate immune sensor PKR. *ACS Chem. Biol.* **11**, 1118–1127 (2016).
12. Wieland, M. & Fussenegger, M. Engineering molecular circuits using synthetic biology in mammalian cells. *Annu. Rev. Chem. Biomol. Eng.* **3**, 209–234 (2012).
13. Lee, C. H., Han, S. R. & Lee, S. W. Therapeutic applications of group I intron-based trans-splicing ribozymes. *Wiley Interdiscip. Rev. RNA* **9**, e1466 (2018).

14. Zhan, X. et al. The structure and catalytic mechanism of a pseudoknot-containing hammerhead ribozyme. *Nat. Commun.* **15**, 6628 (2024).
15. Felletti, M., Stifel, J., Wurmthaler, L. A., Geiger, S. & Hartig, J. S. Twister ribozymes as highly versatile expression platforms for artificial riboswitches. *Nat. Commun.* **7**, 12834 (2016).
16. Ausländer, S., Fuchs, D., Hürlemann, S., Ausländer, D. & Fussenegger, M. Engineering a ribozyme cleavage-induced split fluorescent aptamer complementation assay. *Nucleic Acids Res.* **44**, e94 (2016).
17. Chen, C. C. & Lupták, A. Hunting for human ribozymes. *Nat. Chem. Biol.* **17**, 507–508 (2021).
18. Weinberg, C. E., Weinberg, Z. & Hammann, C. Novel ribozymes: discovery, catalytic mechanisms, and the quest to understand biological function. *Nucleic Acids Res.* **47**, 9480–9494 (2019).
19. Blount, K. F. & Uhlenbeck, O. C. The structure-function dilemma of the hammerhead ribozyme. *Annu. Rev. Biophys. Biomol. Struct.* **34**, 415–440 (2005).
20. Boehr, D. D., Nussinov, R. & Wright, P. E. The role of dynamic conformational ensembles in biomolecular recognition. *Nat. Chem. Biol.* **5**, 789–796 (2009).
21. Dohno, C., Kimura, M. & Nakatani, K. Restoration of ribozyme tertiary contact and function by using a molecular glue for RNA. *Angew. Chem. Int. Ed. Engl.* **57**, 506–510 (2018).
22. Mao, J., DeSantis, C. & Bong, D. Small molecule recognition triggers secondary and tertiary interactions in DNA folding and hammerhead ribozyme catalysis. *J. Am. Chem. Soc.* **139**, 9815–9818 (2017).
23. de la Peña, M., Dufour, D. & Gallego, J. Three-way RNA junctions with remote tertiary contacts: a recurrent and highly versatile fold. *Rna* **15**, 1949–1964 (2009).
24. Hatzakis, N. S. Single molecule insights on conformational selection and induced fit mechanism. *Biophys. Chem.* **186**, 46–54 (2014).
25. Lipfert, J. et al. Double-stranded RNA under force and torque: similarities to and striking differences from double-stranded DNA. *Proc. Natl. Acad. Sci. USA* **111**, 15408–15413 (2014).
26. Yu, Z. et al. Tertiary DNA structure in the single-stranded hTERT promoter fragment unfolds and refolds by parallel pathways via cooperative or sequential events. *J. Am. Chem. Soc.* **134**, 5157–5164 (2012).
27. Li, N. et al. The dynamics of forming a triplex in an artificial telomere inferred by DNA mechanics. *Nucleic Acids Res.* **47**, e86 (2019).
28. Neupane, K. et al. Structural dynamics of single SARS-CoV-2 pseudoknot molecules reveal topologically distinct conformers. *Nat. Commun.* **12**, 4749 (2021).
29. Chandra, V., Hannan, Z., Xu, H. & Mandal, M. Single-molecule analysis reveals multi-state folding of a guanine riboswitch. *Nat. Chem. Biol.* **13**, 194–201 (2017).
30. Greenleaf, W. J., Frieda, K. L., Foster, D. A., Woodside, M. T. & Block, S. M. Direct observation of hierarchical folding in single riboswitch aptamers. *Science* **319**, 630–633 (2008).
31. Zhao, M. & Woodside, M. T. Mechanical strength of RNA knot in Zika virus protects against cellular defenses. *Nat. Chem. Biol.* **17**, 975–981 (2021).
32. Walder, R. et al. High-precision single-molecule characterization of the folding of an HIV RNA hairpin by atomic force microscopy. *Nano Lett.* **18**, 6318–6325 (2018).
33. Onoa, B. et al. Identifying kinetic barriers to mechanical unfolding of the T. thermophila ribozyme. *Science* **299**, 1892–1895 (2003).
34. Pley, H. W., Flaherty, K. M. & McKay, D. B. Three-dimensional structure of a hammerhead ribozyme. *Nature* **372**, 68–74 (1994).
35. Chen, H., Giese, T. J., Golden, B. L. & York, D. M. Divalent metal ion activation of a guanine general base in the hammerhead ribozyme: insights from molecular simulations. *Biochemistry* **56**, 2985–2994 (2017).
36. Mir, A. et al. Two divalent metal ions and conformational changes play roles in the hammerhead ribozyme cleavage reaction. *Biochemistry* **54**, 6369–6381 (2015).
37. Osborne, E. M., Ward, W. L., Ruehle, M. Z. & DeRose, V. J. The identity of the nucleophile substitution may influence metal interactions with the cleavage site of the minimal hammerhead ribozyme. *Biochemistry* **48**, 10654–10664 (2009).
38. Lee, T. S. et al. Role of Mg2+ in hammerhead ribozyme catalysis from molecular simulation. *J. Am. Chem. Soc.* **130**, 3053–3064 (2008).
39. McDowell, S. E., Jun, J. M. & Walter, N. G. Long-range tertiary interactions in single hammerhead ribozymes bias motional sampling toward catalytically active conformations. *RNA* **16**, 2414–2426 (2010).
40. Martick, M. & Scott, W. G. Tertiary contacts distant from the active site prime a ribozyme for catalysis. *Cell* **126**, 309–320 (2006).
41. Kim, N. K., Murali, A. & DeRose, V. J. Separate metal requirements for loop interactions and catalysis in the extended hammerhead ribozyme. *J. Am. Chem. Soc.* **127**, 14134–14135 (2005).
42. Ma, K. et al. A DNA force circuit for exploring protein-protein interactions at the single-molecule level. *Chin. J. Chem.* **42**, 1456–1464 (2024).
43. Wang, Z. et al. Reading time and DNA sequence preference of TET3 CXXC domain revealed by single-molecule profiling†. *Chin. J. Chem.* **41**, 1177–1184 (2023).
44. Yu, Z. et al. A force calibration standard for magnetic tweezers. *Rev. Sci. Instrum.* **85**, 123114 (2014).
45. Collin, D. et al. Verification of the Crooks fluctuation theorem and recovery of RNA folding free energies. *Nature* **437**, 231–234 (2005).
46. Huang, J. et al. CHARMM36m: an improved force field for folded and intrinsically disordered proteins. *Nat. Methods* **14**, 71–73 (2017).
47. Hess, B., Kutzner, C., van der Spoel, D. & Lindahl, E. GROMACS 4: Algorithms for Highly Efficient, Load-Balanced, and Scalable Molecular Simulation. *J. Chem. Theory Comput.* **4**, 435–447 (2008).
48. Brooks, B. R. et al. CHARMM: the biomolecular simulation program. *J. Comput. Chem.* **30**, 1545–1614 (2009).
49. Zhou, J. M. et al. Existence of efficient divalent metal ion-catalyzed and inefficient divalent metal ion-independent channels in reactions catalyzed by a hammerhead ribozyme. *Nucleic Acids Res.* **30**, 2374–2382 (2002).
50. Scott, W. G., Finch, J. T. & Klug, A. The crystal structure of an all-RNA hammerhead ribozyme: a proposed mechanism for RNA catalytic cleavage. *Cell* **81**, 991–1002 (1995).
51. Canny, M. D. et al. Fast cleavage kinetics of a natural hammerhead ribozyme. *J. Am. Chem. Soc.* **126**, 10848–10849 (2004).
52. Hub, J. S., Groot, B. L. D. & Spoel, D. V. D. g_wham—A free weighted histogram analysis implementation including robust error and autocorrelation estimates. *J. Chem. Theory Comput.* **6**, 3713–3720 (2010).
53. Savinov, A. & Block, S. M. Self-cleavage of the glmS ribozyme core is controlled by a fragile folding element. *Proc. Natl. Acad. Sci. USA* **115**, 11976–11981 (2018).

Acknowledgements

This work was supported by the National Natural Science Foundation of China [Grant 32071227 and 32471274 to Z.Y.; 21877065 and 82111530210 to Y.J.L.; 12275137 to Y.L.], Tianjin Municipal Natural Science Foundation of China (22JCYBJC01070 to Z.Y.; 21JCZDJC00260 to Y.J.L.), State key laboratory of precision measuring technology and instruments (Tianjin University) [Grant pilab2210 to Z.Y.].

Author contributions

Z.Y., Y.J.L., and Y.L. conceived, designed, and supervised the experiments; M.L., Z.C., L.X., and H.D. performed the experiments and analyzed the data; K.M. and Y.Q. maintained the single-molecule instruments; S.B.C. and J.H.C. contributed reagents and materials; N.L. created art illustration; M.L., L.X., Y.L., and Z.Y. wrote the paper.

Competing interests

The authors declare no competing interests.

Additional information

Supplementary information The online version contains supplementary material available at https://doi.org/10.1038/s42003-025-07600-3.

Correspondence and requests for materials should be addressed to Yao Li, Yijin Liu or Zhongbo Yu.

Peer review information *Communications Biology* thanks Jekyung Ryu, Jun Fan and the other, anonymous, reviewer(s) for their contribution to the peer review of this work. Primary Handling Editors: Min Zhuang and Dario Ummarino. A peer review file is available.